Supporting Information

Elucidation of Active Sites in Aldol Condensation of Acetone over Single-Facet Dominant Anatase TiO_2 (101) and (001) Catalysts

Fan Lin,[†] Huamin Wang,*[,†] Yuntao Zhao,[†] Jia Fu,[‡] Donghai Mei,*[,†,‡] Nicholas R. Jaegers,[†,§] Feng Gao,[†] Yong Wang*[,†,§]

† Institute for Integrated Catalysis, Pacific Northwest National Laboratory, Richland, Washington 99354, USA

‡ School of Chemistry and Chemical Engineering, Tiangong University, Tianjin 300387, China

§ The Gene and Linda Voiland School of Chemical Engineering and Bioengineering, Washington State University, Pullman, Washington 99164, USA

*Corresponding authors: huamin.wang@pnnl.gov, dhmei@tiangong.edu.cn, yong.wang@pnnl.gov

S1. Synthesis of single facet dominant anatase TiO_2 (101) and TiO_2 (001) model catalysts and Cu/SiO_2 co-catalysts

Facet-selective anatase TiO_2 nanocrystals were synthesized hydrothermally involving two steps: precursor preparation and crystal growth. The catalyst precursor was first prepared by heating the mixture of KOH (Sigma-Aldrich, ≥ 85wt%)solution and TiO_2(P25) at 473 K, and then dried at 353 K overnight.[1] The {101} facet dominant anatase TiO_2, denoted as TiO_2 (101), was prepared by adding 0.2 g of precursor to 180 cm^3 ultrapure water and sonicating the mixture for 30 min. The pH of the mixture was then adjusted to 5.0 by adding 0.1 M HNO_3 (Sigma-Aldrich, ACS reagent, 70%) drop-wise. The resulting synthesis solution was sealed into a 125 cm^3 Teflon-lined stainless steel autoclave (~60 cm^3 in each) and maintained at 473 K for 48 h. The {001} facet dominant anatase TiO_2, denoted as TiO_2 (001), was prepared by adding 0.25 g precursor to 250 cm^3 ultrapure water and sonicating for 45 min. The preferential growth of {001} facet was achieved by adding 45 g of urea (Sigma-Aldrich, ACS reagent) to the solution as a capping agent. The pH of the mixture was adjusted to 13 by gradually adding ~40 cm^3 of KOH (0.3 M). The resulting solution was again sealed into an autoclave and heated at 473 K for 20 h. The as-synthesized catalysts were washed 5 times using ultrapure water, separated by centrifugation, and dried in air at 353 K overnight. The samples were then treated in static air at 823 K for 4 h for impurity removal and structural stabilization.

The Cu/SiO_2 catalyst (~20 wt. % Cu), was prepared using a homogeneous deposition–precipitation method. Colloidal silica (30 wt.%, 21.8 g, LUDOX SM-30), Cu $(NO_3)_2$•$2.5H_2O$ (99.99%, 6.0 g, Sigma-Aldrich), and urea (99%, 4.7 g, Aldrich) were mixed in deionized water (~100 mL). The suspension pH was adjusted to 2-3 using a HNO_3 solution (63 wt. %, Fisher Chemical) and then heated to 363 K (10 K min^{-1}) in a flask and held for 20 h with stirring (10 Hz). The powders were recovered by vacuum filtration and washed with deionized water until the filtrate pH was 7, treated in ambient stagnant air at 383 K for 20 h, and then heated in flowing dry air (200 cm^3 min^{-1}, Zero Grade, Oxarc) to 723 K (at 10 K min^{-1}) and held for 5 h. These samples were treated in flowing 10% H_2/Ar (Ultra High Purity Grade, Oxarc) by heating to 573 K (at 2 K min^{-1}) and held for 2 h, and passivated in flowing 1% O_2/He mixtures (Oxarc) at ambient temperature for 1 h before exposure to ambient air.

S2. Estimation of the number of remaining Lewis acid sites during catalytic rate measurements

In the catalytic rate measurement at a constant temperature (503-533 K), the rates at a specific given set of condition (acetone and isopropanol pressures) were measured for multiple times throughout the course of an experiment to obtain the catalyst deactivation profile. The kinetic model for catalyst deactivation is described by Equation (S1), assuming that the catalyst deactivation is caused by coke deposition and the rate deactivation is proportional to the rate of acetone condensation reaction:

$$r_{\text{per g}_{\text{cat}},t} = \text{TOF} \cdot [\text{L}]_t = r_{\text{per g}_{\text{cat}},0}\exp\left(-k_{\text{d}}t\right) = \text{TOF} \cdot [\text{L}]_0\exp\left(-k_{\text{d}}t\right) \qquad \text{(S1)}$$

where t represents time-on-stream; $r_{\text{per g}_{\text{cat}},t}$ and $r_{\text{per g}_{\text{cat}},0}$ are the rate of acetone condensation in catalyst weight basis at the time-on-stream of t and 0, respectively; TOF is the turnover frequency of acetone condensation; $[\text{L}]_0$ and $[\text{L}]_t$ are the initial Lewis acid site density and the number of Lewis acid site remaining at time-on-stream of t, respectively; k_{d} is the deactivation rate constant at a given condition (temperature and reactant partial pressures). This deactivation profile,

together with the initial Lewis acid site density $[L]_0$, was used to estimate the number of remaining Lewis acid site $[L]_t$ at any time (t) during the experiment.

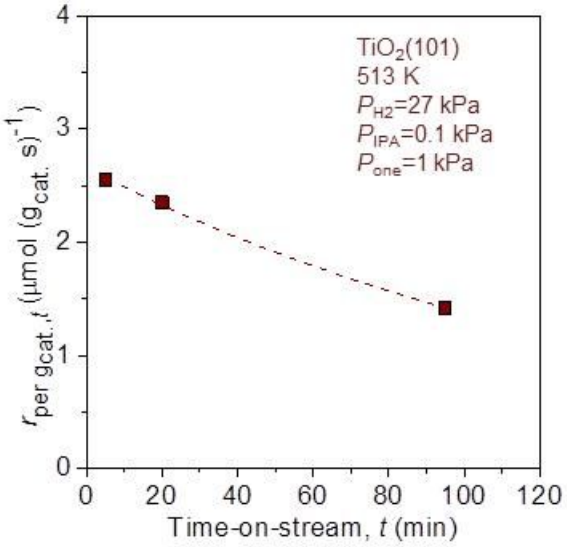

Figure S1. Catalyst deactivation profile: rate of acetone condensation ($r_{\text{per } g_{cat.},t}$, per $g_{cat.}$ basis) on TiO_2 (101)+Cu/SiO_2 (1:2 mass) as a function of time-on-stream (t) (513 K, P_{one}=1 kPa, P_{IPA}=0.1 kPa, P_{H_2}=27 kPa).

S3. Titration of Lewis acid-base site pairs on TiO_2 (101) and TiO_2 (001) model catalysts

The strong interaction of propionic acid with Ti-O site pair allows for the measurement of the Ti-O site pair densities on the TiO_2 catalysts.[2]

We have studied the FTIR spectrum of propanoic acid adsorption on TiO_2(P25) surface. All types of propanoic acid adsorption species observed by FTIR, including those interacting with surface OH groups, confirm that each propanoic acid molecule should poison one Lewis acid site. As shown in Figure S2, on clean TiO_2(P25) surface after pretreatment at 450 ºC in flowing helium, surface OH group still presented at 3715 cm^{-1} (terminal OH) and 3669 cm^{-1} (bridging OH). Upon propanoic acid adsorption, three possible types of adsorption configuration on Lewis acid Ti sites were observed, namely molecular propanoic acid (ν(C=O) at 1665 cm^{-1} and ν(C-O) at 1472 cm^{-1}), monodentate propanoate ($\nu(OCO)_{as}$ at 1540 cm^{-1} and $\nu(OCO)_s$ at 1378 cm^{-1}), and bidentate propanoate ($\nu(OCO)_{as}$ at 1540 cm^{-1} and $\nu(OCO)_s$ at 1440-1420 cm^{-1}).[5] Each of these adsorption configurations occupies one Lewis acidic Ti site, as depicted in Scheme S1. In addition, it was noted that all surface OH groups disappeared due to interaction with propanoic acid. Unlike a perturbing interaction, which would shift OH vibration bands (3669 and 3715 cm^{-1}) to lower frequencies (typically a broad band around 3500cm^{-1}), the complete disappearance of ν(OH) suggests the consumption of OH groups by the esterification-like interaction with propanoic acids.[6-8] We proposed three possible routes of esterification-like interaction between surface OH groups and propanoic acids, as depicted in Scheme S1. Among all the surface species generated, only the ester with free C=O group would not occupy a Lewis acid site. This free C=O group would typically show a stretching vibration band above 1710 cm^{-1},[9] which, however, was not observed in the IR spectrum. Therefore, we can rule out the ester with free C=O groups and confirm that propanoic acid species titrates the Lewis acid sites with a stoichiometric ratio of 1 to

1.

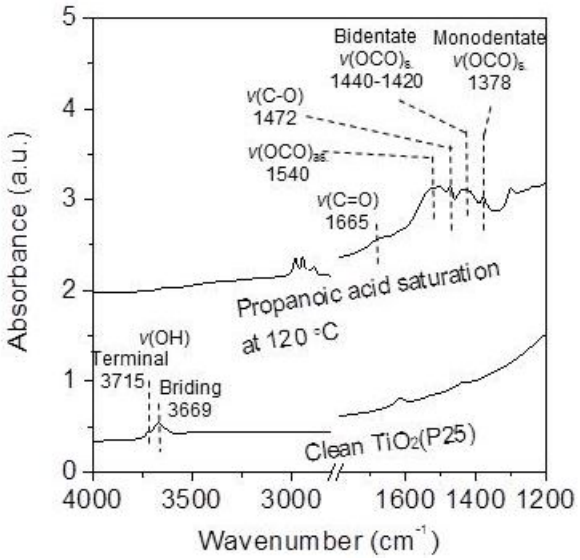

Figure S2. DRIFTS spectra of propanoic acid adsorption on TiO_2(25) at 120 ºC (TiO_2(P25) pretreated at 450ºC in flowing helium).

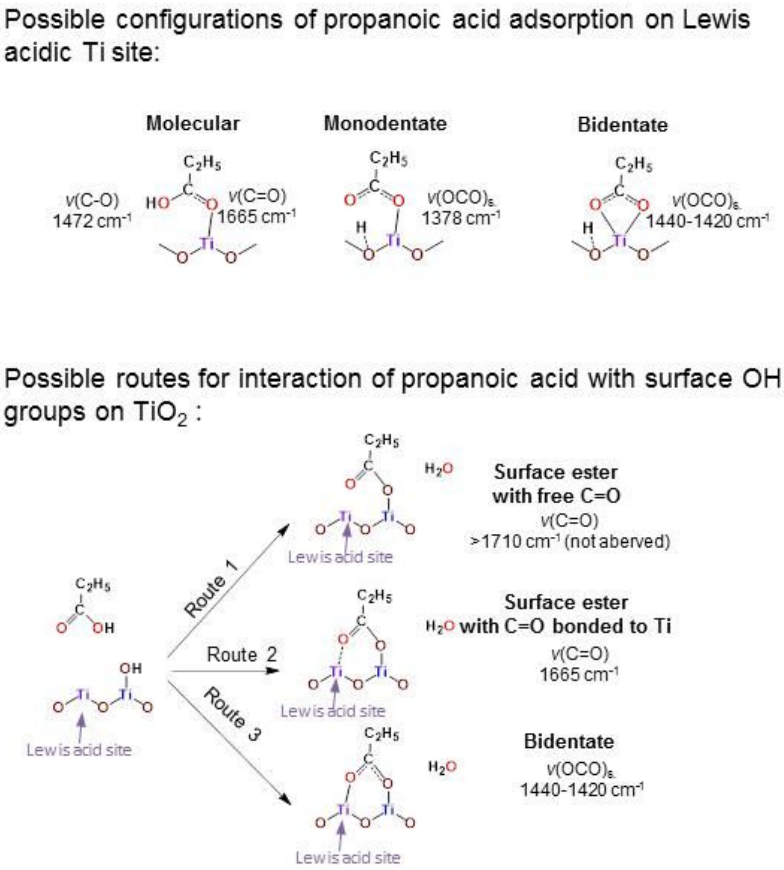

Scheme S1. Possible configurations of propanoic acid adsorption on Lewis acidic Ti site and possible routes for interaction of propanoic acid with surface OH groups on TiO_2.

As shown in Figure S3, after the acetone condensation rate ($r_{C\text{-}C}$) reached steady state at 453 K, introduction of trace amount of propionic acid in the reactant stream led to the decrease of the condensation rates. The amount of propionic acid uptake was determined according to the difference between the concentration of acid in the feed stream (measured prior to introducing on the catalysts) and the total concentration of acid and acid derived product (isopropyl propionate). The acetone condensation rates decreased almost linearly with the amount of propionic acid uptake. As more Ti-O pairs were titrated by propionic acid, slight deviations from these linear trends near the acid saturation point were due to the growing scarcity of vicinal Ti centers, required for C-C coupling steps. It is noted that propanoic acid was not able to fully suppress the acetone condensation, with a small residual activity remaining. This residual activity was likely contributed by the small amount of Brønsted acid sites on the Cu/SiO_2 co-catalysts, which could not be poisoned by propanoic acid. Nevertheless, the influence of this small background activity on the counting of Lewis acid sites is negligible. The linear extrapolation of the deactivation trend to zero $r_{C\text{-}C}$ gave the number of propionic acid titrant required to fully cover the Ti-O site pairs and suppress the acetone condensation reaction, which was also the value of Ti-O site pair density on the TiO_2 catalysts, as listed in Table 1 in the main manuscript.

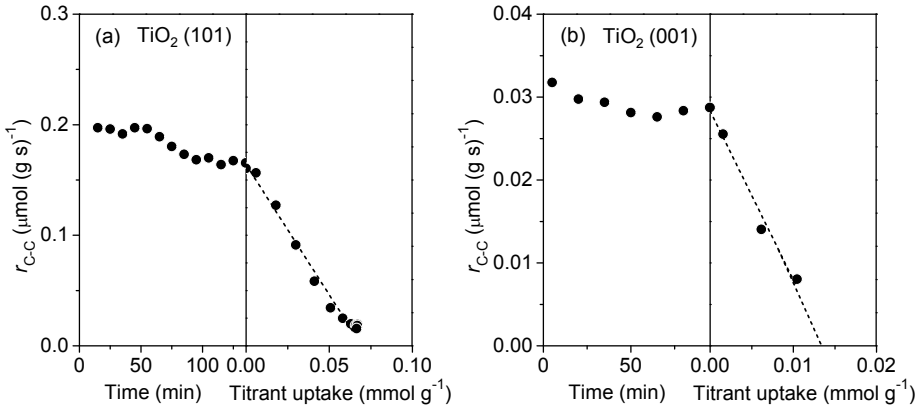

Figure S3. Acetone aldol condensation rates ($r_{C\text{-}C}$) on (a) TiO_2 (101)+Cu/SiO_2 (1:2 mass) and (b) TiO_2 (001)+Cu/SiO_2 (5:1 mass) at 453 K before (vs. time) and after (vs. titrant uptake) the introduction of propionic acid titrant (0.65 kPa acetone, 10 kPa H_2, 3-4 Pa propionic acid).

S4: Co-feeding 2,6-ditertbutyl pyridine to eliminate activity contribution from Bronsted acid sites over Cu/SiO_2

We have ruled out the catalytic contribution from Brønsted acid sites on TiO_2. However, we found that the Cu/SiO_2 co-catalysts contained some Brønsted acid sites, which had minor catalytic contribution to acetone condensation reactions during the kinetic measurements. As shown in Figure S4 for the reaction of acetone+IPA mixtures (4:1 molar ratio) on TiO_2(P25)-Cu/SiO_2 catalysts (1:2 mass), introduction of DTBP slightly decreased the rate of acetone condensation, because DTBP selectively poisoned the Brønsted acid sites on Cu/SiO_2. Although the background catalytic contribution of the Cu/SiO_2 Brønsted acid sites was small, we actually co-fed DTBP to poison the Brønsted acid sites and eliminate their impact on the rate measurements to ensure the measurement accuracy during all the kinetic measurements in the presence of Cu/SiO_2 co-catalysts.

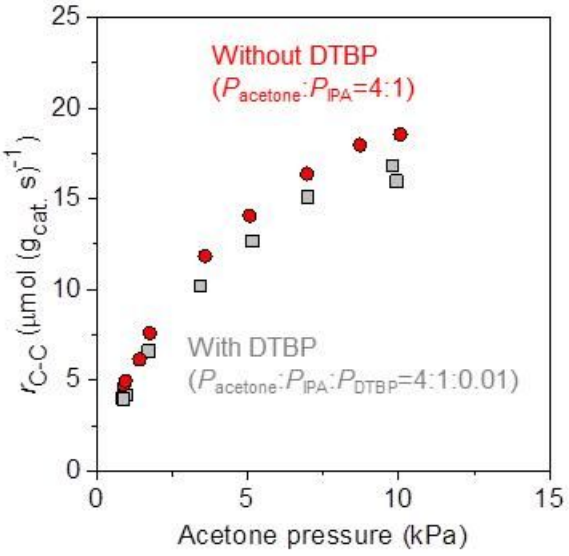

Figure S4. Rate of acetone condensation (r_{C-C}) on TiO_2(P25)+Cu/SiO_2 (1:2 mass) catalysts as a function of acetone pressure in the presence and absence of 2,6-ditertbutyl pyridine (DTBP) (533K, P_{H2}=85 kPa, $P_{acetone}$:P_{IPA}=4:1 or $P_{acetone}$:P_{IPA}:P_{DTBP}=4:1:0.01).

S5. Kinetic isotope effect of acetone-d_6 on aldol condensation

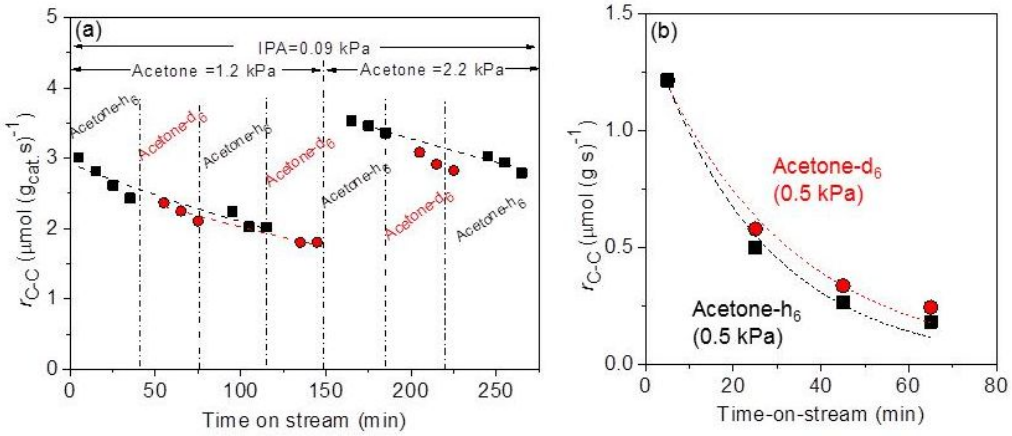

Figure S5. Rates for aldol condensation of acetone-h_6 (black) and acetone-d_6 (red) on TiO_2 (P25) as a function of time-on-stream (a) with acetone-IPA mixture (523 K, IPA pressure=0.09 kPa, acetone pressure=1.2 or 2.2 kPa) and (b) with pure acetone (523 K, acetone pressure=0.5 kPa).

S6. Potential energy profiles and intermediate structures of acetone condensation on pristine {101} facets of anatase TiO_2

Figures S6 shows the DFT calculated potential energy profiles and intermediate structures of acetone condensation on pristine {101} facets of anatase TiO_2. The aldol condensation reaction occurs between two acetone molecules, which adsorb on two vicinal Ti sites. Regarding this mechanism, the transition state for the α-H extraction has the highest energy along the reaction coordinate, making enolation the rate limiting step. This is consistent with the DFT results reported by Wang et al.[2].

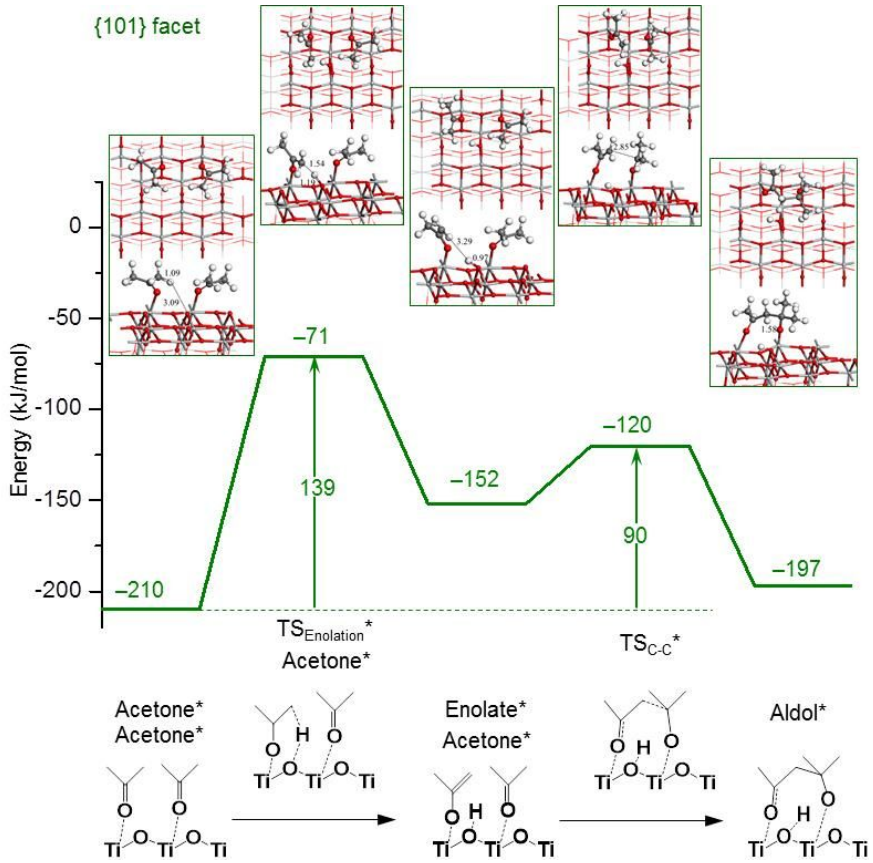

Figure S6. Potential energy profiles and intermediate structures of acetone condensation on pristine {101} facets of anatase TiO_2 (* represents Ti site).

S7. DFT calculation of vibrational frequencies on adsorbed acetone

We calculated the vibrational frequencies of adsorbed acetones over TiO_2 {001} and {101} facets. As shown in Table S1, it is found that DFT calculated vibrational frequencies are largely consistent with the experimentally measured characteristic peaks in the DRIFTS spectra (Figure 5).

Table S1. Comparison of DFT calculated vibrational frequencies with experimental measurements.

Vibrational Frequency (cm^{-1})	**Experiment**	**DFT calculation**	
		TiO_2 {001}	TiO_2 {101}
Acetone adsorbed on the Lewis acid site	1694	1672	1686
Acetone bonded to OH	1707	1707	1699
Terminal hydroxyl groups	3740	3744	3758
Bridging hydroxyl groups	3674	3665	3673
	3694	3706	3694
Interactions between OH and adsorbed acetone	3540	3532	3549

S8. Additional DRIFTS of acetone adsorption under reaction conditions

The most ideal approach to examine the reaction intermediates would be *in-situ* DRIFTS under reaction conditions (temperature and with 2-propanol), if applicable. However, it is extremely difficult to conduct such measurement of steady state acetone condensation reactions on TiO_2 at high temperature (e.g., 523 K) due to fast coke formation. We attempted to carry out the DRIFTS experiments with an acetone-IPA vapor mixture to mitigate catalyst deactivation, similar to the condition of reaction kinetic study (Figure 4). In this case, the coverage of acetone was low, due to the stronger IPA adsorption. In addition, the interference from the vapor phase molecules and adsorbed reaction products made the detection of adsorbed acetone difficult. Nevertheless, we still observed acetone adsorption on both OH group (1707 cm^{-1}) and Ti site (1691 cm^{-1}) before reaching steady state, as shown in Figure S7. It agrees with our DRIFTS results of acetone adsorption and temperature-programmed desorption as well as DFT calculation.

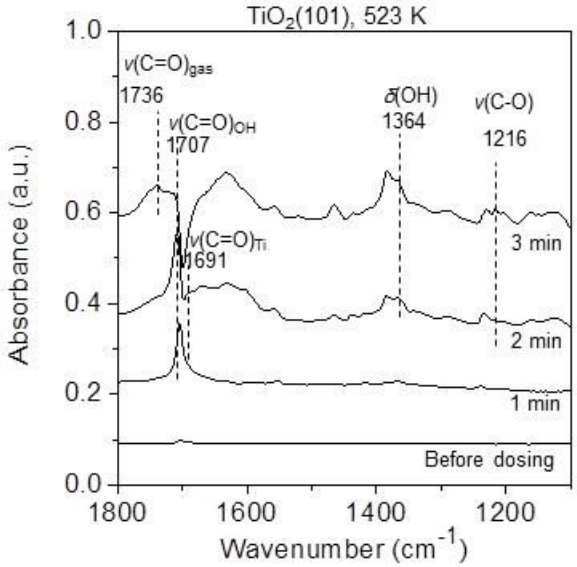

Figure S7. *In-situ* DRIFTS spectra of TiO_2(101) catalyst during the first 3 min of introducing acetone-isopropanol vapor mixture (about 1 to 1 molar ratio) at 473 K.

S9. Additional DFT calculation results on aldol condensation reaction of acetone over the hydroxylated TiO_2 surfaces

Figure S8 shows the optimized structures of aldol condensation reaction of acetone over the hydroxylated TiO_2 {101} and {001} surfaces and Figure S9 shows the overall energy reaction coordinate diagram from initial reactant state to product state.

(a)

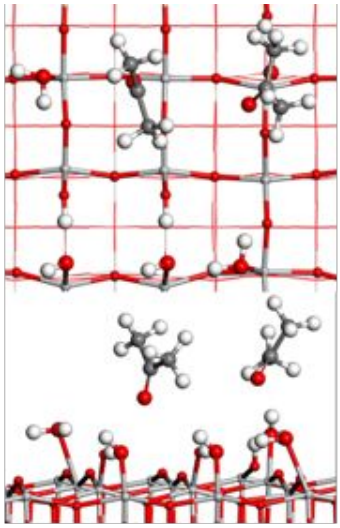

2Acetone(g)
TiO_2(001)-2H_2O-6OH

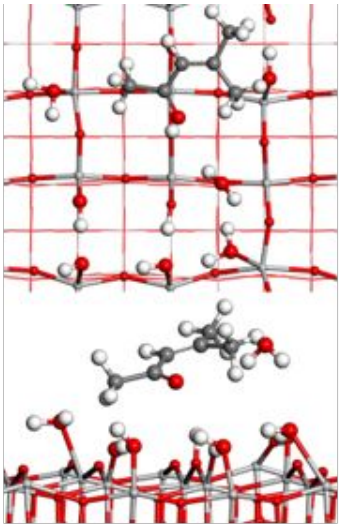

MSO(g) + H_2O(g)
TiO_2(001)-2H_2O-6OH

(b)

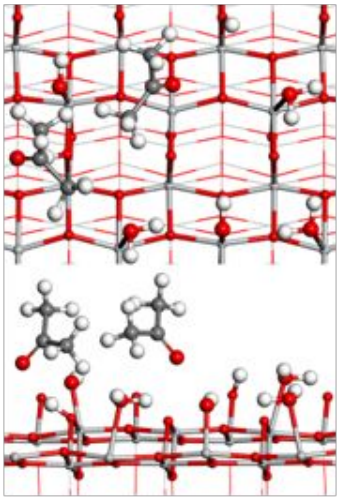

2Acetone(g)
TiO_2(101)-3H_2O-4OH

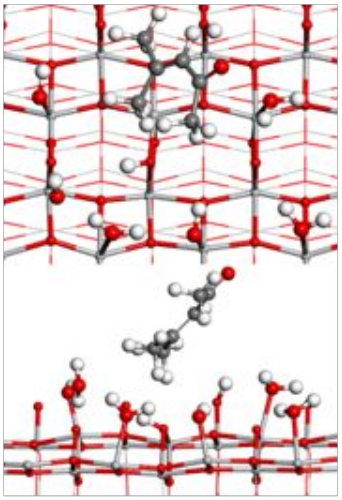

MSO(g) + H_2O(g)
TiO_2(101)-3H_2O-4OH

(c)

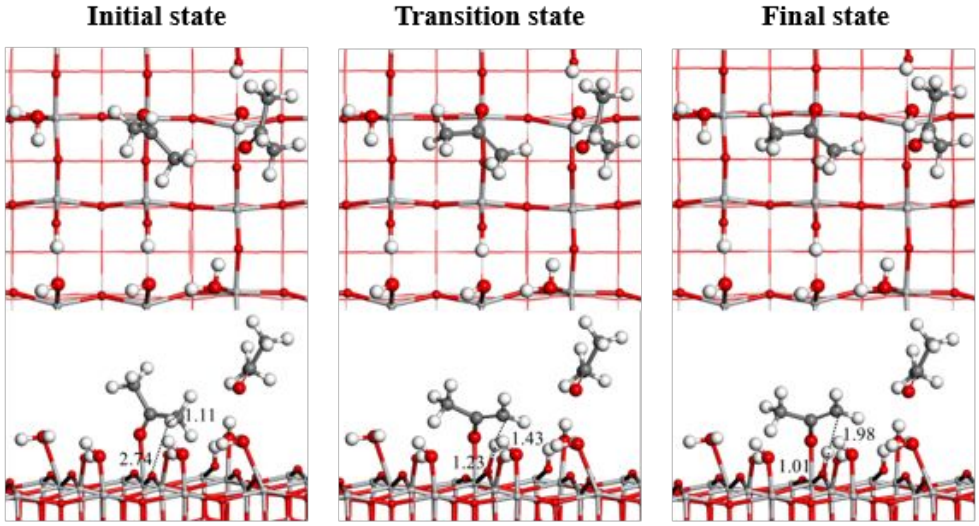

α-H abstraction: Acetone*+Acetone$^{\#}$ +Os→ Enolate*+Acetone$^{\#}$+(Os)H*

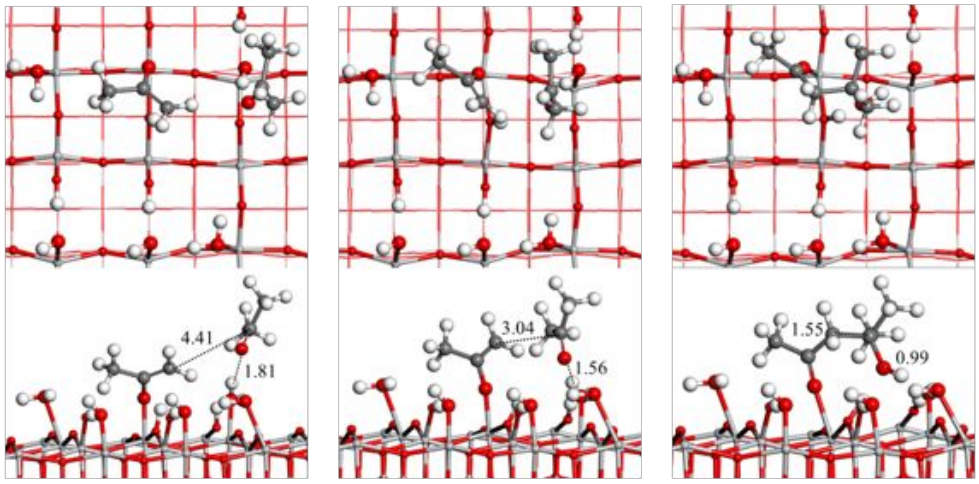

C-C coupling: Enolate*+Acetone$^{\#}$+(Os)H* → Aldol*

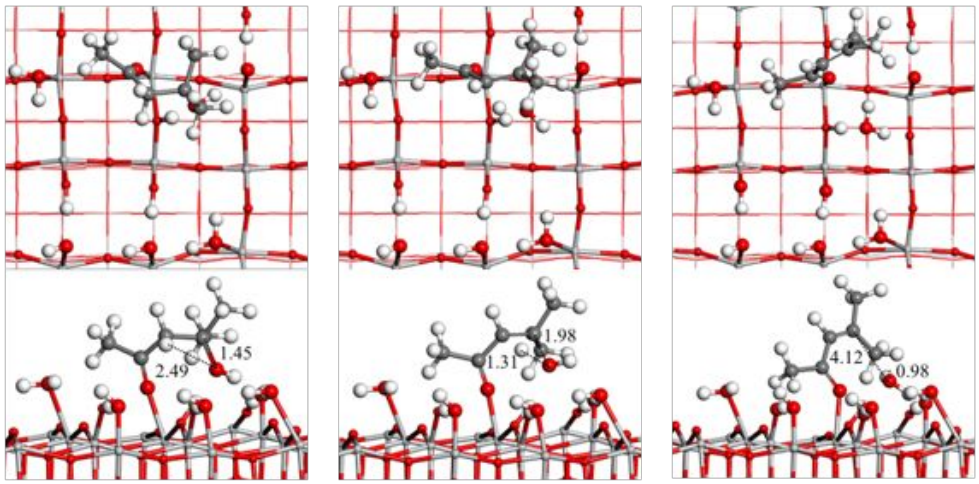

Dehydration: Aldol* → MSO*+H_2O(g)

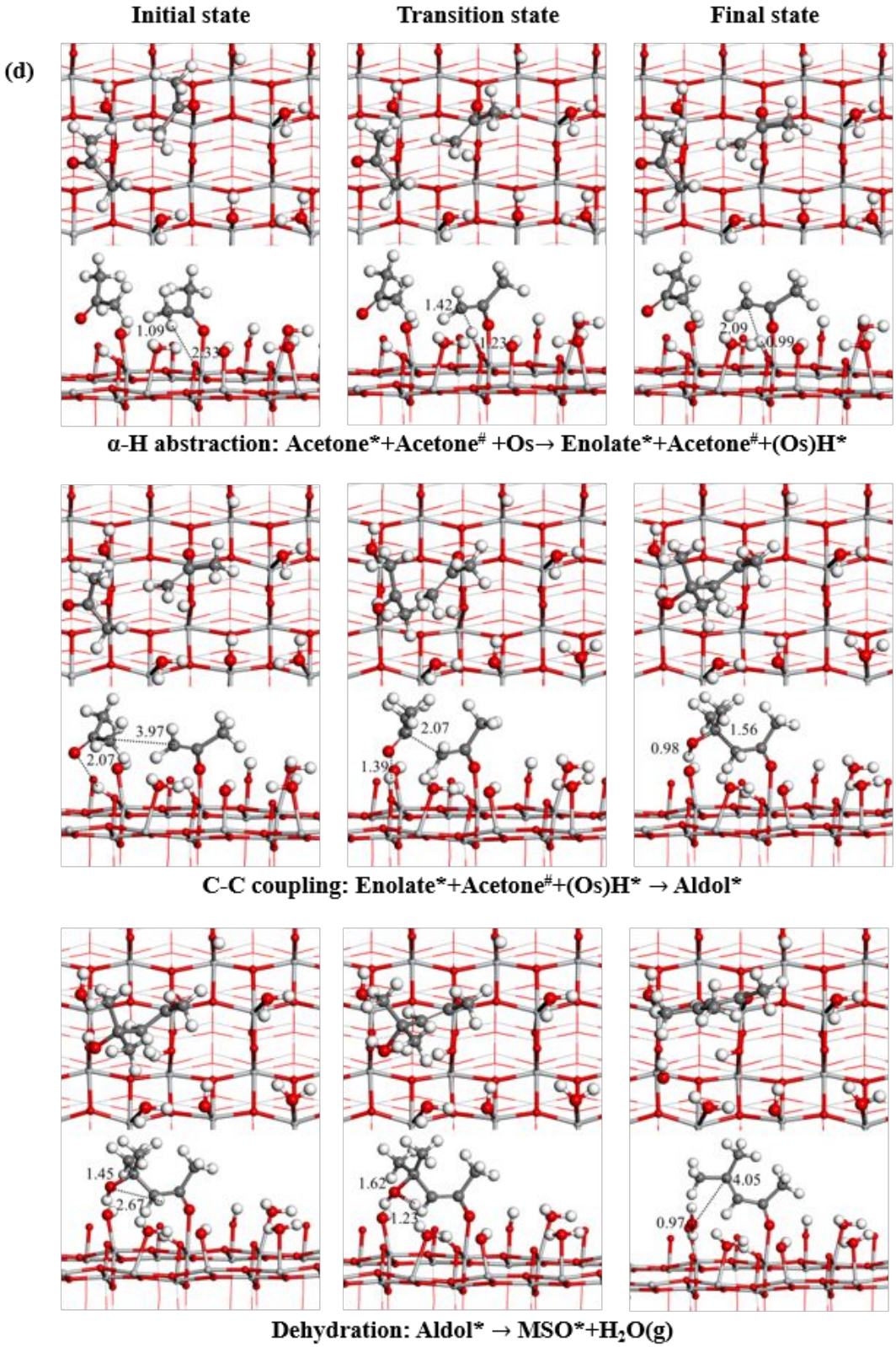

Figure S8. Optimized structures of aldol condensation reaction of acetone over the hydroxylated TiO_2 surfaces (a) and (c) TiO_2 {001} surface; (b) and (d) TiO_2 {101} surface. The top and lower surfaces are top and side view, respectively.

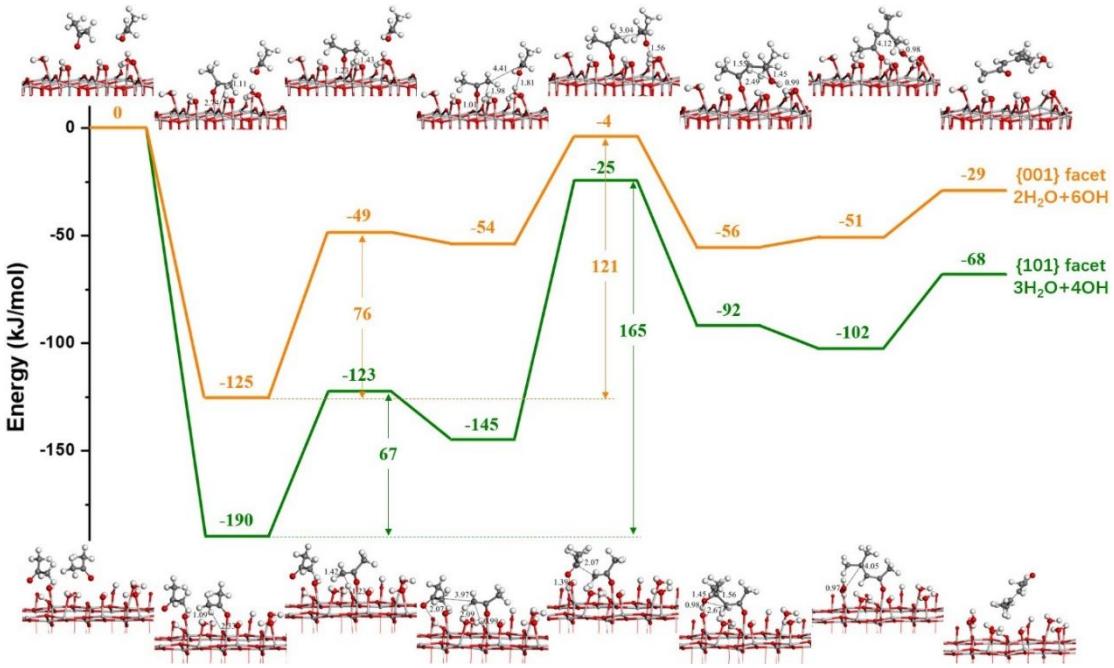

Figure S9. The DFT-derived energy profiles and intermediate structures of acetone condensation on {001} and (b) {101} facet of anatase TiO_2.

We simulated the reaction of two Ti_{5c}-bonded acetones on TiO_2 {101} facet decorated with O_sH groups ($3H_2O$+2OH). The energy profile and the intermediate structures are shown in Figure S10. After one Ti_{5c}-bonded acetone undergoes α-H cleavage to form the Ti_{5c}-bonded enolate, the other Ti_{5c}-bonded acetone attacks the enolate for C-C coupling. As shown by the structure of C-C coupling transition state (TSC-C), when attacking the enolate, the Ti_{5c}-bonded acetone approaches to a surface O_sH group to form the transition state. Again, the C-C coupling has the highest activation barrier, similar to the case of Figure 6 in the main manuscript. This result confirms that in the presence of surface O_sH group, the C-C coupling is more likely occurring between an O_sH-bonded acetone and surface enolate and becoming the kinetically relevant step.

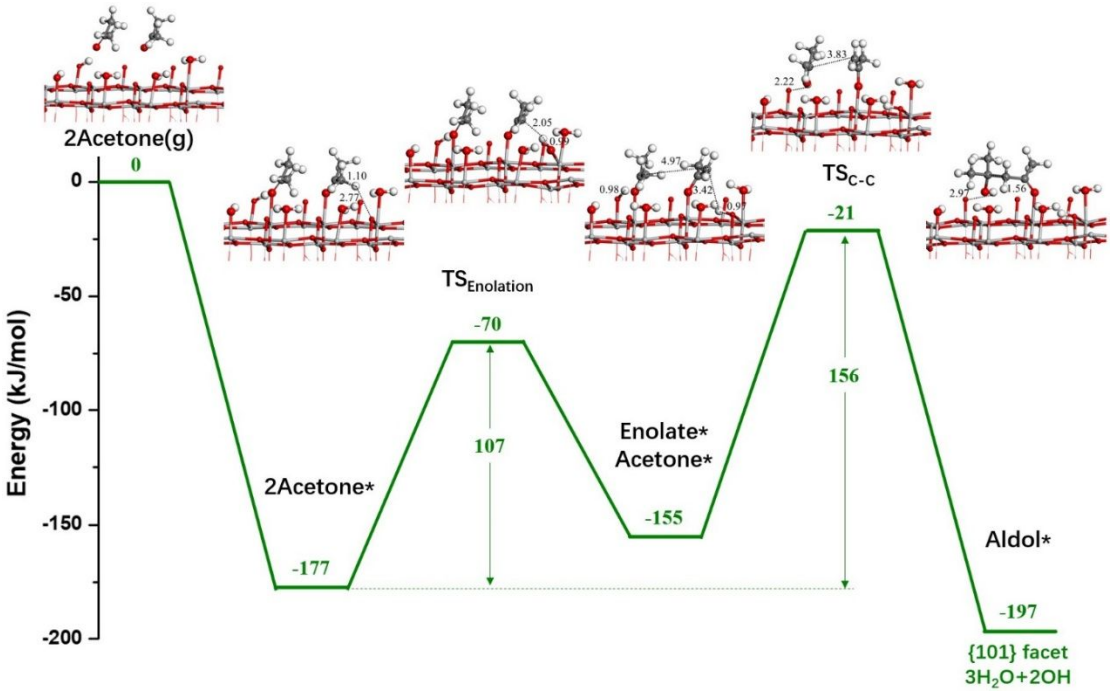

Figure S10. The energy profiles and intermediate structures of acetone condensation on anatase TiO_2 {101} facet with $3H_2O$+2OH.

S10. Kinetic model of acetone condensation on TiO_2 surface populated with OH groups and isopropanol spectators

Scheme S2 depicts the elementary steps, surface intermediates and spectators during acetone condensation on TiO_2 surface populated with O_sH groups. First, acetones adsorb on both Ti site (Step A) and vicinal O_sH group (Step B), with adsorption equilibrium constants of $K_{\mathrm{one-Ti}}$ and $K_{\mathrm{one-OH}}$, respectively. The Ti-bounded acetone can undergo enolation (Step C) forming enolate. Here we assume the reversible enolation step is quasi equilibrated (equilibrium constant K_{Enolate}). The kinetically relevant C-C coupling step proceeds via the nucleophilic attack of the Ti-bounded enolate onto the vicinal O_sH-bounded acetone (Step D, rate constant $k_{\mathrm{C-C}}$), leading to the formation of the aldol product, diacetone alcohol. The rapid dehydration of diacetone alcohol forms mestyl oxide (Step E). In competition to acetone adsorption, isopropanol also adsorbs on both Ti sites and O_sH groups (Steps F and G), with equilibrium constants of $K_{\mathrm{IPA-Ti}}$ and $K_{\mathrm{IPA-OH}}$, respectively. The rate of acetone C-C coupling is expressed as:

$$r_{\mathrm{C-C}} = k_{\mathrm{C-C}} \cdot \frac{K_{\mathrm{Enolate}}K_{\mathrm{one-Ti}}P_{\mathrm{one}}}{1 + K_{\mathrm{one-Ti}}P_{\mathrm{one}} + K_{\mathrm{Enolate}}K_{\mathrm{one-Ti}}P_{\mathrm{one}} + K_{\mathrm{IPA-Ti}}P_{\mathrm{IPA}}} \cdot \frac{K_{\mathrm{one-OH}}P_{\mathrm{one}}}{1 + K_{\mathrm{one-OH}}P_{\mathrm{one}} + K_{\mathrm{IPA-OH}}P_{\mathrm{IPA}}} \quad \text{(S2)}$$

where P_{one} and P_{IPA} denote the partial pressures of acetone and isopropanol, respectively. The terms $K_{\mathrm{one-Ti}}P_{\mathrm{one}}$, $K_{\mathrm{Enolate}}K_{\mathrm{one-Ti}}P_{\mathrm{one}}$, and $K_{\mathrm{IPA-Ti}}P_{\mathrm{IPA}}$ represent the concentrations of adsorbed acetone, enolate, and isopropanaol on Ti sites, respectively, whereas $K_{\mathrm{one-OH}}P_{\mathrm{one}}$ and $K_{\mathrm{IPA-OH}}P_{\mathrm{IPA}}$ represent the concentrations of acetone and isopropanol on O_sH groups, respectively. The DFT calculation results in Figure 6 indicate that the surface enolate is much less stable than the Ti-bounded acetone (with energy differences of 39 and 65 kJ mol^{-1} on {101} and {001} facets, respectively). Therefore, we assume that the concentration of surface enolate is negligible ($K_{\mathrm{Enolate}}K_{\mathrm{one-Ti}}P_{\mathrm{one}} << K_{\mathrm{one-Ti}}P_{\mathrm{one}}$) and Equation (S2) is simplified to:

$$r_{C-C} = \frac{k_{C-C} K_{Enolate} K_{one-Ti} K_{one-OH} P_{one}^{\ 2}}{(1 + K_{one-Ti} P_{one} + K_{IPA-Ti} P_{IPA})(1 + K_{one-OH} P_{one} + K_{IPA-OH} P_{IPA})} \quad \text{(S3)}$$

which is also Equation (2) in the main manuscript. Figures 7a and 7b in the main manuscript and Figure S11 show the rates for acetone condensation (r_{C-C}) on TiO_2 (101) at 503-533K as a function of P_{one}, under P_{IPA}/P_{one} ratios of 1/40, 1/20, 1/10, and 1/5, respectively. The regression of these kinetic data against Equation (2) gave the value of the apparent rate constant $k_{C-C} K_{Enolate}$.

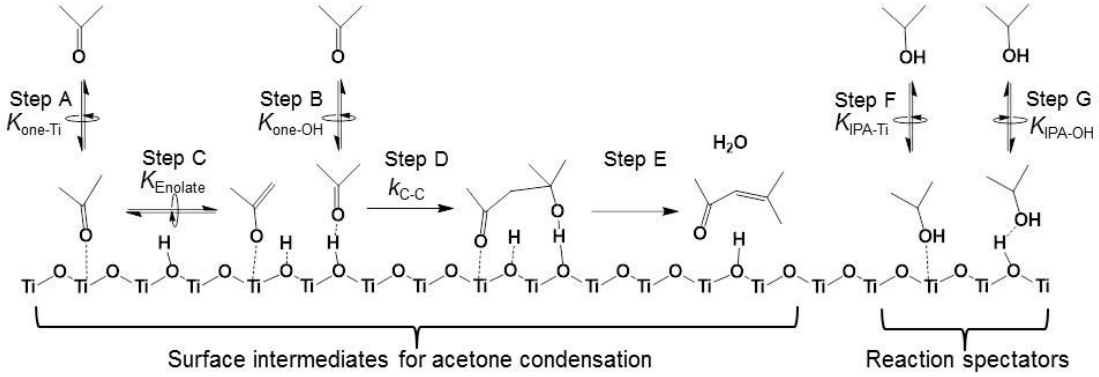

Scheme S2. Proposed reaction steps and adsorption intermediates during the reactions of acetone-isopropanol mixture on anatase TiO_2.

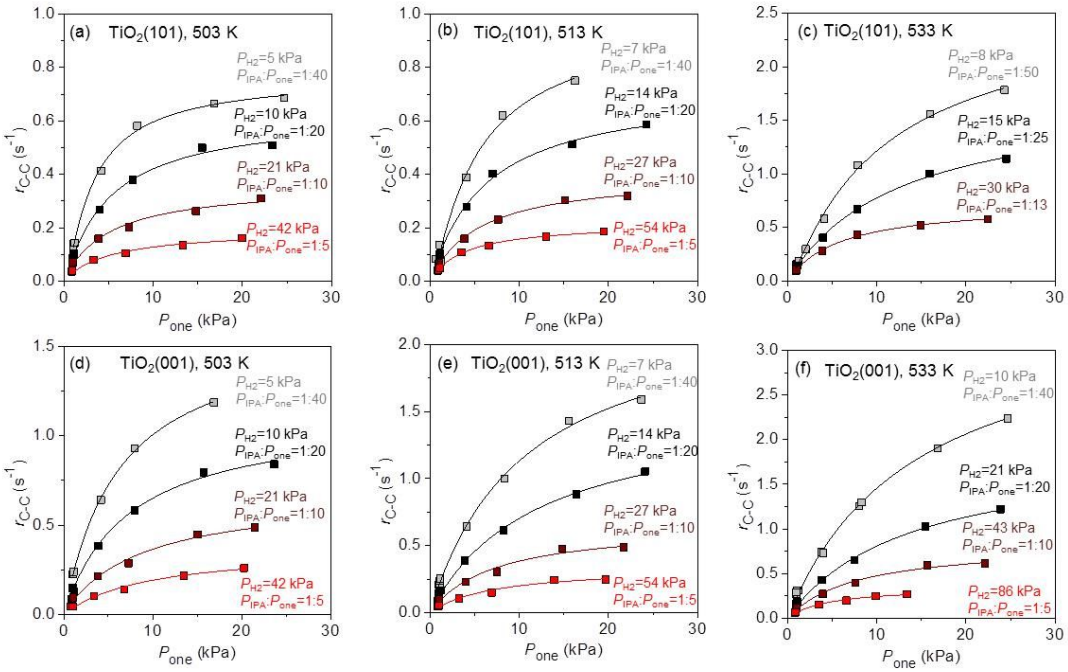

Figure S11. Rates for acetone condensation (r_{C-C}) on TiO_2(101)-Cu/SiO_2 (1:2 mass) or TiO_2(001)-Cu/SiO_2 (1:1 mass) as a function of acetone partial pressure (P_{one}) under constant H_2 partial pressures and constant IPA-to-acetone ratios (P_{IPA}/P_{one}) at different temperatures a) TiO_2 (101), 503 K; b) TiO_2 (101), 513 K; c) TiO_2 (101), 533 K; d) TiO_2 (001), 503 K; e) TiO_2 (001), 513 K; f) TiO_2 (001), 533 K.

S11. Cu/SiO_2 co-catalyst and H_2 do not impact acetone condensation activity on TiO_2

Figures S12 compares the rates of acetone condensation (r_{C-C}) measured in the presence and absence of Cu/SiO_2 co-catalysts and H_2, respectively, under the same temperature (513 K) and P_{IPA}:P_{one} ratio (1/5). In the presence of Cu/SiO_2 co-catalysts and a constant H_2 pressure (P_{H2}=54 kPa), the P_{IPA}/P_{one} ratio of 1/5 was automatically maintained by the acetone-isopropanol hydrogenation equilibrium (Eq. 4 in the main manuscript), regardless of P_{one}. In the absence of Cu/SiO_2 co-catalyst and H_2, P_{IPA} and P_{one} were individually controlled by reactant feeding, and the r_{C-C} measured under the P_{IPA}/P_{one} ratio of 1/5 were picked and plotted. For both TiO_2(101) and TiO_2(001), the data points measured in the absence and presence of Cu/SiO_2 and H_2 basically lay on the same curve, suggesting Cu/SiO_2 and H_2 did not impact the kinetics of acetone condensation on TiO_2.

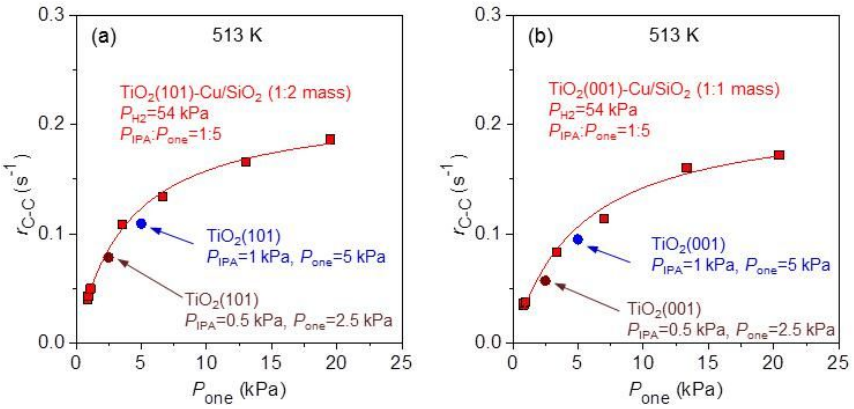

Figure S12. Rates for acetone condensation (r_{C-C}) on (a) TiO_2(101) and (b) TiO_2(001) measured in the presence and absence of Cu/SiO_2 co-catalysts and H_2 (513 K, P_{IPA}:P_{one} =1:5).

References

1. Ye, L.; Mao, J.; Liu, J.; Jiang, Z.; Peng, T.; Zan, L., Synthesis of anatase TiO_2 nanocrystals with {101}, {001} or {010} single facets of 90% level exposure and liquid-phase photocatalytic reduction and oxidation activity orders. *J. Mater. Chem. A* **2013,** *1* (35), 10532-10537.
2. Wang, S.; Goulas, K.; Iglesia, E., Condensation and esterification reactions of alkanals, alkanones, and alkanols on TiO_2: Elementary steps, site requirements, and synergistic effects of bifunctional strategies. *J. Catal.* **2016,** *340*, 302-320.
3. Wang, S.; Iglesia, E., Experimental and Theoretical Evidence for the Reactivity of Bound Intermediates in Ketonization of Carboxylic Acids and Consequences of Acid–Base Properties of Oxide Catalysts. *J. Phys. Chem. C* **2017,** *121* (33), 18030-18046.
4. Qu, Q.; Geng, H.; Peng, R.; Cui, Q.; Gu, X.; Li, F.; Wang, M., Chemically Binding Carboxylic Acids onto TiO2 Nanoparticles with Adjustable Coverage by Solvothermal Strategy. *Langmuir* **2010,** *26* (12), 9539-9546.
5. Zhang, Q.-L.; Du, L.-C.; Weng, Y.-X.; Wang, L.; Chen, H.-Y.; Li, J.-Q., Particle-Size-Dependent Distribution of Carboxylate Adsorption Sites on TiO_2 Nanoparticle Surfaces: Insights into the Surface Modification of Nanostructured TiO_2 Electrodes. *J. Phys. Chem. B* **2004,** *108* (39), 15077-15083.
6. Weng, Y.-X.; Li, L.; Liu, Y.; Wang, L.; Yang, G.-Z., Surface-Binding Forms of Carboxylic Groups on Nanoparticulate TiO2 Surface Studied by the Interface-Sensitive Transient Triplet-State Molecular Probe. *J. Phys. Chem. B* **2003,** *107* (18), 4356-4363.

7. van den Brand, J.; Blajiev, O.; Beentjes, P. C. J.; Terryn, H.; de Wit, J. H. W., Interaction of Ester Functional Groups with Aluminum Oxide Surfaces Studied Using Infrared Reflection Absorption Spectroscopy. *Langmuir* **2004,** *20* (15), 6318-6326.